HHS Public Access

Author manuscript

Mol Microbiol. Author manuscript; available in PMC 2016 February 01.

Published in final edited form as:

Mol Microbiol. 2015 February ; 95(3): 426–441. doi:10.1111/mmi.12867.

Crystal structure of *Bacillus anthracis* virulence regulator AtxA and effects of phosphorylated histidines on multimerization and activity

Troy G. Hammerstrom[1], **Lori B. Horton**[1], **Michelle C. Swick**[1], **Andrzej Joachimiak**[2,3], **Jerzy Osipiuk**[2,3,*], and **Theresa M. Koehler**[1,*]

[1]Department of Microbiology and Molecular Genetics, The University of Texas, Houston Health Science Center at Houston, Houston, TX, USA

[2]Center for Structural Genomics of Infectious Diseases, Argonne, IL, USA

[3]Argonne National Laboratory, Biosciences Division, Structural Biology Center, Argonne, IL, USA

Summary

The *Bacillus anthracis* virulence regulator AtxA controls transcription of the anthrax toxin genes and capsule biosynthesis operon. AtxA activity is elevated during growth in media containing glucose and CO_2/bicarbonate, and there is a positive correlation between the CO_2/bicarbonate signal, AtxA activity, and homomultimerization. AtxA activity is also affected by phosphorylation at specific histidines. We show that AtxA crystallizes as a dimer. Distinct folds associated with predicted DNA-binding domains (HTH1 and HTH2) and phosphoenolpyruvate: carbohydrate phosphotransferase system-regulated domains (PRD1 and PRD2) are apparent. We tested AtxA variants containing single and double phosphomimetic (His → Asp) and phosphoablative (His → Ala) amino acid changes for activity in *B. anthracis* cultures and for protein-protein interactions in cell lysates. Reduced activity of AtxA H199A, lack of multimerization and activity of AtxAH379D variants, and predicted structural changes associated with phosphorylation support a model for control of AtxA function. We propose that (1) in the AtxA dimer, phosphorylation of H199 in PRD1 affects HTH2 positioning, influencing DNA-binding; and (2) phosphorylation of H379 in PRD2 disrupts dimer formation. The AtxA structure is the first reported high-resolution full-length structure of a PRD-containing regulator and can serve as a model for proteins of this family, especially those that link virulence to bacterial metabolism.

Keywords

transcription; phosphotransferase; AtxA; phosphorylation; virulence; anthrax

[*]Osipiuk and Koehler are co-corresponding authors: Theresa M. Koehler, Department of Microbiology and Molecular Genetics, University of Texas, Houston Health Science Center, 6431 Fannin St., MSB 1.508, Houston, TX 77030, Theresa.M.Koehler@uth.tmc.edu. Jerzy Osipiuk, Argonne National Laboratory, 9700 S. Cass Ave. #446, Argonne, IL 60439, josipiuk@anl.gov.

Introduction

Bacterial transcription factors containing nucleic acid binding domains and phosphoenolpyruvate phosphotransferase system (PTS) regulation domains (PRDs) are well-established regulators of genes associated with uptake and metabolism of carbohydrates (Stulke *et al.*, 1998). In response to the availability of specific sugars, the PTS, which consists of Enzyme I (EI), HPr, and sugar-specific Enzyme II complexes (EIIA, B, C, and D), phosphorylates histidine residues within the PRDs to affect regulator function. Well-studied PRD-containing regulators include the *Bacillus subtilis* proteins LicT, GlcT, MtlR, and ManR (van Tilbeurgh *et al.*, 2001, Schmalisch *et al.*, 2003, Wenzel & Altenbuchner, 2013, Joyet *et al.*, 2010). These proteins bind specific DNA sequences to activate transcription initiation or bind specific RNA sequences to serve as anti-terminators. The number and positions of phosphorylated histidines within PRDs vary among the regulators, and phosphorylation can positively or negatively affect protein activity. In addition, phosphorylation has been shown to affect the multimeric structure of PRD-containing proteins by stabilizing or destabilizing the protein-protein complex (Graille *et al.*, 2005).

The archetype PRD-containing regulator, LicT, is an anti-terminator that controls expression of genes required for import and metabolism of β-glucosides (Schnetz *et al.*, 1996). LicT is comprised of an amino-terminal RNA-binding domain followed by two PRDs (van Tilbeurgh *et al.*, 2001). HPr phosphorylates H207 and H269 within PRD2 of LicT, while the β-glucoside-specific EIIBCA complex BglP phosphorylates H100 within PRD1 (Tortosa *et al.*, 2001). HPr-dependent phosphorylation of PRD2 promotes dimer formation, resulting in increased LicT activity (Graille *et al.*, 2005). In contrast, phosphorylation of PRD1 decreases LicT activity by destabilizing the dimeric form (Ben-Zeev *et al.*, 2005).

In recent years, genome analyses of Gram-positive pathogens have revealed additional apparent PRD-containing regulators. Some of these proteins are established or predicted transcriptional regulators of virulence genes. The pleotropic virulence regulators AtxA of *Bacillus anthracis* and Mga of *Streptococcus pyogenes* are the best-characterized members of this emerging class of PRD-containing virulence regulators, designated “PCVRs” (Hondorp *et al.*, 2013). Consistent with the overall domain organizations of established PRD-containing regulators (Stulke *et al.*, 1998), AtxA and Mga are predicted to have amino-terminal DNA-binding domains, two central PRDs, and a carboxy-terminal region with amino acid similarity to the PTS protein EIIB (Tsvetanova *et al.*, 2007, Hondorp *et al.*, 2012). The EIIB-like regions of AtxA and Mga are associated with homomeric multimerization (Hammerstrom *et al.*, 2011, Hondorp *et al.*, 2012). For each protein, phosphorylation of histidine residues affects activity, but the numbers and positions of the phosphorylated residues within the PRDs differ (Tsvetanova *et al.*, 2007, Hondorp *et al.*, 2013). The proteins also differ in the numbers of predicted DNA-binding domains; AtxA has two helix-turn-helix motifs while Mga has three such motifs. Although AtxA and Mga have been subjected to extensive *in silico* analysis, there are few reports describing the biochemistry of the proteins. The regulators are somewhat recalcitrant to purification and can be unstable in solution (Hondorp *et al.*, 2012).

Our research group and others have focused on the signals and mechanisms for control of *atxA* gene transcription and consequently, expression of the AtxA regulon. Transcription of *atxA* is affected by temperature, redox potential, growth phase, and the presence of glucose (Chiang *et al.*, 2011, Dai & Koehler, 1997, Saile & Koehler, 2002, Wilson *et al.*, 2009). The transition state regulator AbrB negatively affects *atxA* expression (Saile & Koehler, 2002, Strauch *et al.*, 2005), and other *trans*-acting regulators have also been implicated in *atxA* transcription (Chiang *et al.*, 2011, Dale *et al.*, 2012). Growth of *B. anthracis* in media containing bicarbonate in elevated levels of atmospheric CO_2 affects AtxA activity post-transcriptionally (Dai & Koehler, 1997, Dai *et al.*, 1995, Hammerstrom *et al.*, 2011, Koehler *et al.*, 1994, Sirard *et al.*, 1994). In these culture conditions, which are thought to mimic the mammalian host environment, AtxA positively controls transcription of the three structural genes *lef*, *pagA*, and *cya* for the anthrax toxin proteins, the capsule biosynthetic operon *capBCADE*, and numerous other genes on the *B. anthracis* chromosome and plasmids (Bourgogne *et al.*, 2003). *atxA*-null mutants are highly attenuated in murine models for anthrax (Dai *et al.*, 1995, Dale *et al.*, 2012). Thus, this PCVR is viewed as a critical regulator of *B. anthracis* virulence.

In the current model for AtxA function, protein activity is modulated by phosphorylation at two histidines: H199 in PRD1 and H379 in PRD2 (Tsvetanova *et al.*, 2007). Using AtxA variants with amino acid substitutions that mimic non-phosphorylated and phosphorylated histidines, Tsvetanova and coworkers (Tsvetanova *et al.*, 2007) showed the effects of AtxA phosphorylation on transcription of a *pagA-lacZ* reporter fusion in the heterologous host *B. subtilis.* Expression of *pagA-lacZ* was decreased six-fold by AtxA H199A relative to native AtxA, whereas AtxA H199D had activity comparable to the native protein. In contrast, AtxA H379A showed activity similar to the native protein, but the activity of AtxA H379D was greatly reduced relative to native AtxA. Toxin levels in culture supernates of *B. anthracis* mutants expressing the AtxA variants supported the findings obtained using the *B. subtilis* system. Taken together, the results indicate phosphorylation at H199 in PRD1 facilitates AtxA function while phosphorylation at H379 reduces the activity of the protein (Tsvetanova *et al.*, 2007). AtxA function is also controlled by the carboxy-terminal EIIB-like region of the protein. We reported that a truncated AtxA missing the 91-amino acid C-terminal region is inactive. We showed that the C-terminus is required for protein multimerization and that multimerization is enhanced in conditions known to promote expression of AtxA-regulated genes (Hammerstrom *et al.*, 2011).

Here we report that the crystal structure of AtxA is a dimer with protein-protein contacts at the carboxy-terminal domains. We use strains containing single and double phosphomimetic and phosphoablative mutations to examine relationships between AtxA phosphorylation and multimerization. Our data allow us to make predictions regarding structural implications of phosphorylation. Crystal structures of truncated forms of the PRD-containing regulators GlcT and LicT have provided insight into structure/function relationships of this important familiy of regulators (Himmel *et al.*, 2012, van Tilbeurgh *et al.*, 2001). To the best of our knowledge, the AtxA crystal structure presented here is the first published high-resolution structure of a full-length PRD-containing protein.

Results

The crystal structure of AtxA

The AtxA amino acid sequence suggests two amino-terminal DNA-binding domains, two PRDs, and a C-terminal domain resembling EIIB (Hammerstrom *et al.*, 2011, Tsvetanova *et al.*, 2007), (Fig. 1A). In agreement with these predictions, the AtxA crystal structure is multimodular, with five distinct domains (Fig. 1B). The asymmetric unit of the AtxA crystals contains two monomers of the protein (chain A and chain B). Chain A is significantly better defined in the structure than chain B and consists of the entire protein with exception of residues 273–275. Selected data collection and refinement statistics are provided in Tables S1 and S2, respectively. Associated with each AtxA monomer is an N-dodecyl-β-D-maltoside molecule (Fig. 1B), a non-ionic detergent added during protein crystallization to improve crystal quality. The ligand binds between helices H2, H4 and H5 and appears to stabilize the N-terminal portion of the protein (Fig. S1).

We showed previously that AtxA multimerizes in *B. anthracis* cell lysates and in preparations of purified protein (Hammerstrom *et al.*, 2011). The biological assembly of the protein is a homodimer, molecule A and molecule B, which is in agreement with these biochemical studies. The biological dimer was created using chain A in the structure and its symmetry-related molecule (Fig. 1B). The A–B dimer interface is formed mainly by contacts between helices H20 on PRD2 of molecule A, and H21, on the EIIB-like domain of molecule B (Fig. S2). The key residues responsible for the H20–H21 helix interactions are L375, T382, L386 and N389 from H20 on molecule A and I403, Y407, E413 and K414 from H21 on molecule B. The dimer is symmetrical and the same interactions are repeated between helix H20 of molecule B and helix H21 of molecule A. The Y407 residue of H21 helix additionally stabilizes the dimer by hydrogen bonds with residues R345 and H346 on the H17–H18 loop. The buried area of the dimer is 4720 $Å^2$ compared to 46740 $Å^2$ of total dimer surface area. The free energy of the dimer dissociation is predicted to be 16.9 kcal/M which means that the assembly is thermodynamically stable (based on PISA server (Protein interfaces, surfaces and assemblies service PISA at European Bioinformatics Institute) (Krissinel & Henrick, 2007). The same dimer was observed in two other crystal forms with different space groups, $C222_1$ and $P42_12$, and different crystal packing (data not shown).

The first two domains near the N-terminus of AtxA have structures indicative of DNA-binding. Residues 7–74 of the N-terminal domain form a winged helix-turn-helix motif, (“HTH1” in Fig. 1A, helices H2–H4 in Fig. 1C). The closest structural homolog for this domain is the winged HTH motif in PurR (PDB ID 1P4A, DALI (Holm & Rosenstrom, 2010) Z-score of 8.7), with 2.0 Å RMSD for 66 peptide backbone residues. PurR is a negative regulator of *Bacillus subtilis* that controls genes associated with purine metabolism (Bera *et al.*, 2003). Residues 76–162 of the AtxA structure form a second helix-turn-helix domain (“HTH2” in Fig. 1A), previously designated “Mga-HTH” because it has primary sequence similarity to a predicted domain in the *Streptococcus pyogenes* virulence regulator Mga (McIver & Myles, 2002). The domain consists of 5 α-helices, one 3_{10} helix and two β-strands forming a wing. Three central helices, H6, H7 and H8, form the core HTH2 motif (Fig. 1C). The closest structural homolog is an HTH domain in NolR (PDB ID 4ON0, Z-

score of 8.3 and RMSD of 2.4 Å for 66 residues), a small protein of *Rhizobium* that controls nodulation and symbiosis genes (Lee *et al.*, 2014). The AtxA HTH2 domain structure closely resembles the NolR protein with the exception of the positioning of terminal helices.

The third and fourth AtxA domains are PTS regulation domains (PRDs) (Fig. 1A). Each domain forms an α-helical bundle characteristic of PRD structures with a core of two pairs of antiparallel helices (Fig. 1B). The PRD1 domain is attached to the HTH2 domain by an unstructured linker. The closest structural homolog for both of the AtxA PRDs is LicT, a transcription anti-terminator of *B. subtilis* that regulates genes involved in β-glucoside metabolism (PDB ID 1TLV) (Graille *et al.*, 2005). DALI Z-scores are equal to 11.4 and 10.7, RMSD are 2.4 Å and 3.1 Å for 99 and 107 residues of PRD1 and PRD2, respectively.

The placement of the fifth, C-terminal, domain of AtxA at the dimer interface is consistent with our previous findings indicating that this region of AtxA is required for AtxA-AtxA interaction (Hammerstrom *et al.*, 2011). The overall fold of the C-terminal domain is a four-stranded parallel β-sheet flanked by three α-helices (Fig. 1B), which closely resembles other EIIB structures in proteins of the bacterial phosphotransferase system. The closest structural homolog for the AtxA EIIB-like domain is the C-terminal domain of a putative PRD-containing transcriptional regulator of *Enterococcus faecalis* (J. Osipiuk, R. Wu, S. Moy, A. Joachimiak unpublished results, PDB ID 3SQN) with Z-score of 9.6 and RMSD of 2.3 Å for 77 residues. The domain is also very similar (2.5 Å RMSD) to the EIIB family protein PtxB of *Streptococcus mutans* (PBD ID 3CZC) (Lei *et al.*, 2009).

Effects of phosphomimetic and phosphoablative mutations on AtxA self-association

For many PRD-containing regulators, protein multimerization and activity are affected by phosphorylation of specific histidine residues in the PRDs, yet the locations and numbers of phosphorylated histidines vary. Tsvetanova and coworkers reported phosphorylation of AtxA at histidine residues H199 and H379 (Tsvetanova *et al.*, 2007). The AtxA crystal structure indicates that H199 is located on helix H12 in PRD1 next to the linker between PRD1 and HTH2. H379 is located on helix H20 in PRD2. The residue is buried inside the domain and interacts with helix H16 of the same domain (Fig. 1B, 1C and Fig. 2).

In a previous report, we used co-affinity purification and chemical cross-linking experiments to show the presence of AtxA multimers in *B. anthracis* cell lysates and in purified preparations of His-tagged AtxA (Hammerstrom *et al.*, 2011). To assess potential relationships between AtxA multimerization and phosphorylation, we constructed *B. anthracis* ANR-1 strains expressing epitope-tagged AtxA variants with histidine → aspartic acid (phosphomimetic) and histidine → alanine (phosphoablative) substitutions at H199 or H379 and tested for protein multimerization. Cultures of UT376 (*atxA*-null) strains containing pUTE991 (AtxA-His), pUTE992 (AtxA-FLAG with H199 or H379 mutations), or pUTE1013 (GFP-FLAG) were cultured and induced with IPTG during exponential phase. Samples were collected at transition phase. Cells from cultures producing AtxA-His were mixed with cells from cultures producing FLAG-tagged AtxA variants or FLAG-tagged GFP. Soluble cell lysates generated from the mixed samples were applied to NTA-Ni resin to assess co-affinity purification of FLAG-tagged proteins with His-tagged AtxA.

Figure 3 shows the AtxA variants in samples before ("Load") and after ("Eluate") affinity purification. Immunoblotting with α-His, α-FLAG, and α-AtxA antibodies revealed comparable amounts of the proteins in lysates prior to affinity purification (lanes 1–6). Following elution of His-tagged AtxA (lanes 7–12), co-eluted FLAG-tagged proteins were visualized in immunoblots with α-FLAG antibodies. As expected, AtxA-FLAG co-purified with AtxA-His (lane 8). The variants AtxA H199A-FLAG, AtxA H199D-FLAG, and AtxA H379A-FLAG also co-purified with AtxA-His (lanes 9–11). In contrast, AtxA H379D-FLAG was not visible in samples eluted from the NTA-Ni resin (lane 12), suggesting that phosphorylation at H379 prevents monomers of AtxA from interacting with each other.

We also tested for AtxA-AtxA interaction in cell lysates using chemical cross-linking. We reported previously that the cysteine-reactive agent bis(maleimido) hexane (BMH) covalently links two AtxA molecules and that crosslinking is dependent upon C402 in the EIIB domain (Hammerstrom *et al.*, 2011). Soluble cell lysates containing His-tagged AtxA variants were treated with BMH and subjected to western blotting (Fig. 4). Upon crosslinking with BMH, we observed a form of AtxA with an apparent size consistent with that of a homodimer (lane 2). Immunoreactive bands of similar size were visible in lanes 3–5, 7, and 9, indicating that AtxA H199A, AtxA H199D, AtxA H379A, AtxA H199A/H379A, and AtxA H199D/H379A form multimers comparable to native AtxA. Conversely, the only band observed for AtxA H379D, AtxA H199A/H379D, and AtxA H199D/H379D corresponded to proteins of ~50 kDa, the size of monomeric AtxA (lanes 6, 8, and 10). Consistent with the results from our co-affinity purification experiments, AtxA variants with the H379D modification did not appear to self-interact. These data indicate that the H379D mutation destabilizes AtxA-AtxA interaction, while H379A, H199A, and H199D do not affect AtxA multimerization.

In vivo activity of AtxA phosphomimetic and phosphoablative variants

We employed *B. anthracis* strains harboring single and double H199 and H379 mutants and the transcriptional reporter P*lef-lacZ* to quantify the *in vivo* activity of AtxA variants. Culture samples were collected as described for the cross-linking experiments. As shown in Figure 5, the H199A mutation resulted in an approximately 6-fold decrease in AtxA activity, while the H199D mutation resulted in activity comparable to that of native AtxA. Aspartic acid and alanine substitutions at H379 had the reverse affect; H379A retained activity, while H379D activity was barely detectable, indicating that this mutant was severely impaired for function. Analysis of the double mutants revealed that the effect of the H379D modification was dominant; activity of H199A/H379D and H199D/H379D was comparable to the single H379D variant. Finally, the increased activity of the H199D/H379A compared to that of H199A/H379A suggests that phosphorylation at H199 is important for function when AtxA can dimerize. These results are in agreement with a previous study assessing AtxA activity in the heterologous host *B. subtilis* (Tsvetanova *et al.*, 2007). Moreover, our results assign unique roles to each histidine for control of AtxA function.

Because the H379D mutation had a dramatic effect on AtxA multimerization and activity, we sought to examine the activity of additional AtxA variants harboring H379 substitutions. We generated a set of H379 variants covering a range of side chain volumes and charges and

repeated the cross-linking and transcriptional activity assays. As shown in Figure 6, substitutions A, Q, S, and K allowed for AtxA dimer formation comparable to that seen with the native protein, despite their very different side chain characteristics. Conversely, the D and E substituted mutants, both standard phosphomimetic mutations (Wittekind *et al.*, 1989, Casabon *et al.*, 2009) showed sharp decreases in the abundance of the dimer while maintaining a prominent monomer band. The A, Q, S, and K variants also displayed wild-type levels of activity at the *lef* promoter (Fig. 7), while the D and E variants displayed no activity. Taken together, these data suggest that the decreased activities observed for the H379D and H379E phosphomimetic mutants are specifically due to changes in protein function caused by the charge, not the size, of the amino acid at position 379. Furthermore, the results support the model for decreased AtxA multimerization and activity associated with phosphorylation of H379.

Effects of phosphomimetic mutations on capsule production

To determine if AtxA control of capsule synthesis mirrors its control of the *lef* promoter, we tested for the presence of capsule on cells of strains containing the AtxA variants. We created Ames strains (pXO1+ pXO2+) in which the native *atxA* locus was deleted, and then complemented *in trans* with *atxA* alleles encoding H199 and H379 variants. The strains were cultured in conditions conducive for capsule synthesis. Cells from late exponential phase cultures were mixed with India ink and examined using a light microscope. As shown in Figure 8, cells of the *atxA*-null mutant produced little to no capsule as expected (Drysdale *et al.*, 2004), whereas complementation of the *atxA*-null mutation with native AtxA resulted in robust capsule production. The capsule phenotypes of the AtxA H199A/H379D and H199D/H379D mutants matched that of the *atxA*-null mutant; cells were mostly nonencapsulated, with rare cells covered by a very thin capsule. Capsule synthesis by the AtxA H199A/H379A strain was slightly more apparent, with more cells covered by a thin capsule. In contrast to the other mutants, all cells of the AtxA H199D/H379A mutant were encapsulated, with capsule thickness approaching that of the strain harboring native AtxA. Overall, capsule production by the mutants was consistent with the phenotypes observed for expression of the toxin reporter, *lef-lacZ* (Fig. 5). The data suggest that phosphorylation of AtxA at H379 negatively affects capsule production while phosphorylation at H199 promotes activity.

Discussion

The AtxA crystal structure in combination with our results revealing the dimerization state of AtxA phosphomimetic and phosphoablative variants and our quantitative assessment of AtxA activity *in vivo*, allow us to make predictions regarding the structural effects of AtxA phosphorylation. Tsvetanova and coauthors first reported phosphorylation of AtxA (Tsvetanova *et al.*, 2007). They showed that AtxA activity is abolished in H379D variants, and the activity of AtxA H199A is reduced relative to native AtxA and AtxA H199D. In our previously published work, we demonstrated that AtxA multimerizes. We showed that AtxA deletion constructs missing the C-terminal EIIB-like domain do not multimerize and are inactive. In addition, we established a positive correlation between AtxA multimerization

and activity; the AtxA dimer to monomer ratio is elevated in cells cultured in conditions conducive for AtxA activity (Hammerstrom *et al.*, 2011).

The data presented here show that while multimerization is unaffected in the AtxA H199 variants, AtxA H379D does not interact with other AtxA monomers, indicative of a prominent role for H379 phosphorylation in control of AtxA activity by impairing dimerization. The AtxA crystal structure, which was obtained using non-phosphorylated protein purified from recombinant *Escherichia coli*, shows H379 located on helix H20 of PRD2 with the side chain extending toward helix H16, also on PRD2 (Fig. 2A and 2C). A hydrogen bond between H379 NE2 and F312 main-chain O, as well as π-stacking of the side chains, likely stabilize the helix H20 - helix H16 interaction. Despite helix H20 involvement in dimer formation, there are no close contacts between H379 and the partner AtxA molecule in the protein dimer. The local environment of H379 is crowded and the only possibility for addition of a phosphoryl group to the histidine is on the dimer interface side. Phosphorylation would require a change of the histidine rotamer to move the side chain from the helix H16 - helix H20 plane to the domain surface. The rotation would presumably push I403 of helix H21 of the opposite molecule and subsequently push the entire helix H21 away. The increased distance between the H20 and H21 helices of the paired subunits would weaken their interaction. Thus, it is reasonable to hypothesize that phosphorylation would destabilize dimer formation depending almost solely on H20–H21 helix interaction.

Phosphorylation of H199, located in PRD1, affects AtxA function; the activity of AtxA H199A is 5- to 7-fold lower than that of native AtxA and AtxA H199D. Yet, multimerization is unaffected by phosphorylation at this residue. The AtxA crystal structure shows that H199 is adjacent to the linker between PRD1 and the HTH2 domain (Fig. 2A and 2B). The NE2 atom of the histidine is positioned to form hydrogen bonds with main-chain oxygen atoms of P164, N165 and Y167, tethering the linker to PRD1 and indirectly stabilizing the relative positions of the two domains. Phosphorylation of H199 would introduce a negative charge on the PRD1 surface. This phosphorylation event is predicted to result in a significant change in the linker-PRD1 interaction by introducing changes in the size and charge. Phosphohistidine at position 199 would disrupt hydrogen bonds and physically move the linker away from PRD1. Alternatively, a different rotamer of H199 would place the phosphate group on the protein surface without a physical contact to the linker. This side chain repositioning would remove hydrogen bonds between the linker and unphosphorylated H199 that apparently stabilize HTH2-PRD1 positioning. Thus, the H199 phosphorylation may change the relative position of the HTH2 and PRD1 domains, potentially affecting HTH2-DNA interaction.

Taken together, the lack of dimerization and activity of the AtxA H379D and H379E variants, the reduced activity of AtxA H199A, and predictions of structural changes associated with phosphorylation at these residues support a model in which AtxA is active as a dimer, and AtxA structure and function is regulated by its phosphorylation state. We propose distinct roles for each phosphorylation event. In the AtxA dimer, phosphorylation at H199 of PRD1 affects positioning of HTH2 and enhances DNA binding activity. Phosphorylation at H379 of PRD2 prevents H20–H21 helix interaction, altering the position of the EIIB domain, and disrupting or destabilizing the AtxA dimer.

AtxA positively controls expression of the anthrax toxin genes, the capsule biosynthetic operon, and a number of other genes on the *B. anthracis* plasmids and chromosome (Bourgogne *et al.*, 2003). AtxA has been proposed to be a transcription activator, yet there are no reports of specific DNA-binding activity of the protein and in our hands AtxA associates with DNA nonspecifically *in vitro* (unpublished data). The adjacent HTH1 and HTH2 domains of the AtxA structure suggest a DNA-binding function for the regulator, supporting its function as an activator. We have attempted to deduce the AtxA DNA-binding sites from known DNA-protein complex structures. Although PurR is the closest structural homolog of the AtxA HTH1 domain, the structure of the PurR-DNA complex is not known. Thus, we used another homolog of HTH1, the *E. coli* response regulator KdpE (PBD ID 4KNY) (Narayanan *et al.*, 2014). KdpE, like AtxA, does not have a well-defined consensus sequence for DNA-binding, and appears to bind primarily AT-rich DNA, such as the DNA found in the control regions of *B. anthracis* genes (Hadjifrangiskou & Koehler, 2008, Njoroge *et al.*, 2012). The superposition of AtxA-HTH1 and KdpE (Fig. S3) indicates binding of helix H4 inside the DNA major groove and wings interacting with the DNA minor groove. The NolR-DNA complex (PBD ID 4ON0) (Lee *et al.*, 2014) offers a model for DNA binding and the AtxA HTH2 domain. NolR is a global regulator of nodulation and symbiosis gene expression in rhizobia, and recognizes variable asymmetric operator sites in the control regions of these genes (Lee *et al.*, 2014). Using NolR as a model, AtxA helix H8 is inside the DNA major groove (Fig. S4). At the same time, the AtxA HTH1 domain is located proximally to the major groove next to the HTH2 domain. Only small adjustments of domain orientations would be necessary for simultaneous DNA binding by the HTH1 and HTH2 domains.

The DNA-binding model based on the NolR-DNA structure shows acceptable fit of a single DNA molecule bound to both HTH motifs in the AtxA monomer, however, the DNA strands bind separately to the two molecules in the AtxA dimer represented in the crystal structure and the strands point in significantly different directions (Fig. S5). Thus DNA binding would require extensive DNA bending. This model is in agreement with our previous investigations of DNA target curvature. We reported *in silico* and *in vitro* analyses indicating that AtxA-controlled promoters display intrinsic curvature, suggesting that local DNA conformation may contribute to DNA-binding specificity (Hadjifrangiskou & Koehler, 2008). Interestingly, target DNA curvature may also be important for DNA-binding by Mga of *Streptococcus pyogenes* and by MgaSpn, a *Streptococcus pneumoniae* PCVR that has a predicted domain organization similar to that of AtxA and Mga (Hondorp & McIver, 2007, Solano-Collado *et al.*, 2013, Tsvetanova *et al.*, 2007). A consensus DNA sequence for Mga-binding has been proposed, but Mga-binding sites have low sequence identity (McIver *et al.*, 1995). MgaSpn has been shown to interact with a specific DNA sequence in the promoter region of a target gene, but upon binding the regulator forms mutimeric complexes that spread along the flanking DNA (Solano-Collado *et al.*, 2013).

An alternative model for AtxA dimer - DNA interaction would require a relocation of the HTH domains. The conformation of the AtxA dimer represented in our crystal structure may be specific for the unphosphorylated protein in the absence of a DNA molecule. Multi-domain proteins like AtxA may change conformation around inter-domain linkers in

response to protein modifications and/or interactions with ligands. The structures of unphosphorylated and phosphorylated LicT protein showed that histidine phosphorylation of the PRDs leads to significant domain movement (Graille *et al.*, 2005, van Tilbeurgh *et al.*, 2001). Similar conformation changes may occur in phosphorylated AtxA such that both molecules bind DNA without a need for substantial DNA bending. We are currently attempting co-crystalization of the AtxA variant proteins with DNA fragments from the control regions of the anthrax toxin genes.

Comparison of the AtxA structure to that of 3SQN, a functionally uncharacterized PRD-containing regulator of *Enterococcus faecalis*, (J. Osipiuk, R. Wu, S. Moy, A. Joachimiak unpublished results, 3SQN PDB deposit) also provides insight into a possible model for DNA binding. The two proteins share only 21.1% amino acid sequence identity but have remarkably similar domain order and arrangement. Each AtxA domain has a close structural and functional counterpart in the *E. faecalis* protein. Although the relative orientations of the first three domains are similar for both structures, orientations along the PRD1-PRD2 and PRD2-EIIB-like domains diverge (Fig. S6). Surprisingly, the two HTH motifs of the *E. faecalis* protein structure align almost perfectly for DNA binding. A superposition of the *E. faecalis* protein and the NolR - DNA structure shows near perfect fitting of the protein DNA-binding helices into the DNA major groove (Fig. S7). Moreover, DNA strands bound to dimer subunits are nearly coaxial and would accommodate a single, double-stranded DNA helix with minimal distortion. Unfortunately, there are currently no reports regarding the function of the *E. faecalis* protein.

Assessment of AtxA structure and function allows us to consider similarities and differences between AtxA and other PRD-containing transcriptional regulators for which relationships between phosphorylation, dimerization, and activity have been discerned. For LicT of *B. subtilis*, when activating phosphohistidines are mutated to aspartic acid residues, the protein dimerizes and becomes constitutively active (Tortosa *et al.*, 2001). Aspartic acid substitutions at non-activating histidines destabilize the LicT dimer and reduce activity (Mignot *et al.*, 2003, Sirard *et al.*, 2000, Cachat *et al.*, 2008). For regulators MtlR and LicR, when phosphohistidines that down-regulate activity are mutated to non-phosphorylatable residues, protein activity is greatly increased in non-inducing conditions (Tobisch *et al.*, 1999, Joyet *et al.*, 2010). Interestingly, in the case of AtxA, none of the AtxA variants displayed activity greater than that of the native protein.

Mga, the best-studied homologue of AtxA, differs from AtxA in the number and locations of phosphohistidines. Unlike AtxA, which contains one phosphohisitidine in each PRD, Mga harbors two phosphohistidines in its PRD1 and one phosphohistidine in its PRD2. As is true for AtxA, phosphorylation affects multimerization and activity of Mga, but only the PRD1 phosphohistidines have been implicated in protein function. A doubly phosphorylated PRD1 phosphomimetic variant of Mga does not form homomultimers and does not activate transcription. Interestingly, Mga variants disrupted for phosphorylation at both PRD1 residues (Mga PRD1 AA and DD variants) are attenuated in a group A streptococcus virulence model (Hondorp *et al.*, 2013).

PTS-regulated domains, “PRD”s, are so-named because their function is controlled via the PTS. Mga is phosphorylated by the PTS phosphotransfer protein HPr *in vitro* (Hondorp *et al.*, 2013) and, like other PRD-containing regulators, the Mga regulon includes sugar metabolism operons and *ccpA*, which mediates carbon catabolite repression (Ribardo & McIver, 2006). In contrast, a clear relationship between AtxA and the PTS has not been established. The AtxA regulon does not contain genes with obvious ties to carbohydrate metabolism (Bourgogne *et al.*, 2003), and one report suggests that *atxA* transcription, rather than AtxA function, is controlled by catabolite repression (Chiang *et al.*, 2011).

Interestingly, Tsvetanova and coworkers (Tsvetanova *et al.*, 2007) detected phosphorylated AtxA H199 and AtxA H379 during growth in rich medium, a condition in which the AtxA-controlled toxin genes are expressed at a relatively low level (Bartkus & Leppla, 1989). For our measurements of AtxA activity, we cultured our strains in a semi-defined medium containing 0.8% sodium bicarbonate and incubated the cultures in air with 5% CO_2, conditions that are conducive for high-level expression of the AtxA-controlled toxin genes (Bartkus & Leppla, 1989, Cataldi *et al.*, 1992, Sirard *et al.*, 1994, Fouet & Mock, 1996, Dai *et al.*, 1995, Koehler *et al.*, 1994). The relative amounts of di-phosphorylated, mono-phosphorylated, and non-phosphorylated AtxA during growth in different conditions are not known and the mechanism for CO_2/bicarbonate - enhanced AtxA function has not been determined. The 72 water molecules evident in the AtxA structure do not appear to represent either carbon dioxide or bicarbonate. Future work will address the influence of specific growth conditions, including elevated CO_2/bicarbonate, on the phosphorylation state of AtxA, and the factors(s) required for phosphorylation.

Many established PRD-containing regulators contain a C-terminal domain with similarity to soluble domains of EII proteins the sugar-specific permeases of the PTS. The placement of the EIIB-like domains of each AtxA molecule in the dimer structure is in agreement with our previous investigations indicating that the C-terminal region of AtxA is required for AtxA-AtxA interaction (Hammerstrom *et al.*, 2011). We reported that AtxA can be cross-linked as a dimer using bis(maleimido) hexane (BMH), a reagent that cross-links available cysteines within 13 Å (Hammerstrom *et al.*, 2011). Our data showed that C402 of the EIIB domain is required for crosslinking by BMH and our experiments using Cys → Ser variants suggested that this crosslinking required C402 on both molecules. The crystal structure does not reveal cysteines located within 13 Å of C402, indicating that a change in protein conformation would be required for intermolecular crosslinking by BMH. It is notable that the crystal structure of 3SQN, the uncharacterized PRD-containing protein of *E. faecalis*, does not contain a cysteine residue analogous to AtxA C402. There are only 3 cysteines in the 3SQN - all located in the PRD1 domain and distant from the dimer interface. However, 3SQN residue P407, which resides in a position comparable to C402 of AtxA, does not appear to be within 13 angstroms of the same residue of the opposite chain. AtxA may exist in at least two states, an open state represented by the crystal structure and a closed state represented by the cross-linked dimer.

In summary, this work is the first reported crystal structure of a PRD-containing virulence regulator (PVCR). While AtxA phosphorylation and structure are in line with those of archetype transcriptional regulators that are controlled by the PTS, there is currently no

direct evidence for PTS-mediated phosphorylation of AtxA. Future work will address the role of the PTS in AtxA function and will include studies of the specific signals that may affect AtxA phosphorylation. PTS-controlled transcription factors were first identified in the well-studied, non-pathogenic, soil bacterium *Bacillus subtilis*. As more genome sequences have become available, and as *in silico* analyses have been refined, this family of regulators has grown to include genes/proteins with known or predicted roles in virulence gene expression. Investigations of relationships between virulence gene expression and metabolic signals, such as the presence of specific sugars, will add another dimension to host-pathogen signaling.

Experimental procedures

Strains and culture conditions

Bacillus anthracis strains and plasmids are shown in Table 1. The virulent Ames strain (pXO1+ pXO2+), and the Ames mutant UTA22 were used for capsule experiments. The attenuated Ames non-reverting (ANR-1) strain (pXO1+ pXO2-) and isogenic mutants were employed for all other studies. *B. anthracis* spores were inoculated into Luria-Bertani (LB) (Bertani, 1951) or Brain Heart Infusion (BHI) broth and incubated at 30°C with shaking (200 rpm) for 8 h. Unless otherwise noted, cultures were diluted into Casamino Acid (CA) broth (Thorne & Belton, 1957) containing 0.8% dissolved sodium bicarbonate to an initial OD_{600} density of approximately 0.08 (Hammerstrom *et al.*, 2011). CA cultures were grown at 37°C in 5% atmospheric CO_2 with shaking (200 rpm), and monitored for optical density ($O.D._{600}$) through stationary phase. To induce expression of *atxA* from the hyper-spank promoter, 10–40 μM IPTG was added to the culture two hours after diluting the cells in CA medium. *E. coli* strains TG-1 (Sambrook, 2001) and JM109 (Yanisch-Perron *et al.*, 1985) were used as hosts for cloning. *E. coli* strains were cultured in LB at 37°C with shaking. *E. coli* strains carrying the temperature-sensitive pHY304 vector were cultured at 30°C. Antibiotics were added as appropriate: spectinomycin (100 μg/ml for *B. anthracis* and 50 μg/ml for *E. coli*), erythromycin (5 μg/ml for *B. anthracis* and 150 μg/ml for *E. coli*), ampicillin (100 μg/ml), and carbenicillin (100 μg/ml).

DNA isolation and manipulation

Cloning experiments employing *E. coli* strains JM109 and TG1 were conducted using standard protocols. Plasmid DNA was isolated from *E. coli* using a Zyppy Plasmid Miniprep kit (Zymo Research, Irvine, CA) according to the manufacturer's protocol. *E. coli* strain GM2163 (*dam dcm* mutant) was used to generate unmethylated plasmid DNA for electroporation of *B. anthracis* (Marrero & Welkos, 1995). DNA was amplified by the PCR using KOD (Novagen, Madison, WI), Onetaq, or Phusion polymerase (New England Biolabs, Ipswich, MA). Oligonucleotide primers are described in Table S3. PCR products were purified using a DNA Clean & Concentrator-5 kit (Zymo Research). Restriction enzymes and T4 ligase were purchased from New England Biolabs. Chromosomal DNA was purified using a Mo Bio genomic isolation kit (Mo Bio Laboratories, Solana Beach, CA).

Construction of *B. anthracis* mutants

B. anthracis strain UTA22 was constructed as a markerless gene deletion mutant. The markerless deletion was created using pHY304, a temperature-sensitive vector harboring an erthyromycin-resistance gene. Primers JR170-171 and JR172-173 were used to amplify 1-kb regions upstream and downstream of *atxA*, respectively. The amplicons were fused via overlap-extension PCR and inserted into pHY304 using restriction enzymes *Sac*II and *Exo*I. Following sequence verification of the cloned DNA, the plasmid was electroporated into the Ames strain. A resulting transformant was cultured as described previously (Pflughoeft *et al.*, 2011) to allow for two independent single crossover recombination events, thus excising the *atxA* gene. Resulting isolates were screened for erthyromycin sensitivity, indicating loss of the plasmid. Deletion of the gene was confirmed by sequencing the locus.

Plasmid construction

To create a vector for expression in *E.coli* and purification of AtxA with an amino-terminal His_6-tag (His_6-AtxA), DNA encoding full-length AtxA protein was amplified from pUTE991 using primers AtxA F and AtxA R (Table S3) and cloned into pMCSG68, a derivative of the vector pMCSG53 (Eschenfeldt *et al.*, 2013). Both plasmids are available from the DNASU plasmid repository (https://dnasu.org). The resulting construct, pJOP2, was transformed into *E. coli* BL21[DE3] (Shuman, 1989).

To create *B. anthracis* strains producing AtxA variants with amino acid changes, the AtxA expression vector pUTE658, which contains the IPTG-inducible promoter hyper-spank, was used as a template. To generate each mutant allele, point mutations in the *atxA* gene were created using overlap-extension PCR with primers TH195, TH196, and the appropriate forward and reverse mutagenic primers (Table S3) (Horton *et al.*, 1989). Where noted, phosphoablative and phosphomimetic mutants were tagged with a His_6 epitope on the C-terminus using primers TH195 and TH199 and the mutant pUTE658 plasmids as templates. In all cases, mutations were confirmed by DNA sequencing. Plasmids encoding parent and AtxA variants were electroporated individually into *B. anthracis* strain UT376 (*atxA*-null) with selection for spectinomycin-resistance (Hammerstrom *et al.*, 2011).

Purification and crystallization of His_6-AtxA

The vector encoding His_6-AtxA was transformed into *E. coli* BL21[DE3] for expression and purification. Cells were cultured in M9 medium supplemented with ampicillin. A selenomethionine (SeMet) derivative of the expressed AtxA protein was prepared as described by Walsh et al. (Walsh *et al.*, 1999). Cells were harvested by centrifugation, disrupted by sonication, and the insoluble cellular material was removed by centrifugation. AtxA protein was purified from other contaminating proteins using Ni-NTA (Qiagen, Germantown, MD) affinity chromatography with the addition of 5 mM β-mercaptoethanol in all buffers. The protein was digested with 0.15 mg TEV protease per 20 mg purified protein for 16 h at 4°C, and then passed through a Ni-NTA column to remove both the TEV protease and cleaved N-terminal tag. The final step of purification was gel-filtration on HiLoad 16/60 Superdex 200 pg column (GE Healthcare, Piscataway, NJ) in 10 mM HEPES buffer pH 7.5, 500 mM NaCl and 1 mM DTT. The protein was concentrated on Amicon Ultracel 30K centrifugal filters (Millipore, Billerica, MA) to a concentration of 26 mg/ml.

AtxA crystallization

The initial crystallization condition was determined with a sparse crystallization matrix at 4°C and 16°C using the sitting-drop vapor-diffusion technique using MCSG crystallization suite (Microlytic, Burlington, MA), Pi-minimal and Pi-PEG screens (Gorrec *et al.*, 2011) (Jena Bioscience, Jena, Germany). The best crystals were obtained from B6 conditions of Pi-PEG screen (0.91 M lithium sulfate, 0.15 M cacodylate buffer pH 6.5, 0.14 M potassium bromide) at 4°C. The additive screen (Hampton Research, Aliso Viejo, CA) was used to test improvement of crystallization. Only N-dodecyl β-D-maltoside, a detergent, was found to improve crystal X-ray diffraction. AtxA with addition of the detergent was submitted for crystallization with all original screens again. The best crystals were obtained from F2 conditions of MCSG2 screen at 4°C (3 M sodium chloride, 0.1 M Bis-Tris buffer pH 6.5, 0.2% n-Dodecyl β-D-maltoside). Crystals selected for data collection were soaked in the crystallization buffer supplemented with 25% glycerol and flash-cooled in liquid nitrogen.

AtxA Crystal Data Collection, Structure Determination, and Refinement

Single-wavelength X-ray diffraction data were collected at 100 K temperature at the 19-ID beamline of the Structural Biology Center (Rosenbaum *et al.*, 2006) at the Advanced Photon Source at Argonne National Laboratory using the program SBCcollect. The intensities were integrated and scaled with the HKL3000 suite (Minor *et al.*, 2006).

The structure was determined by single-wavelength anomalous dispersion (SAD) phasing using AutoSol Wizard from PHENIX suite (Adams *et al.*, 2002). Several rounds of manual adjustments of structure models using COOT (Emsley & Cowtan, 2004) and refinements with Refmac program (Murshudov *et al.*, 1997) from CCP4 suite (Collaborative Computational Project, 1994) were done. The stereochemistry of the structure was validated with PHENIX suite (Adams *et al.*, 2002) incorporating MOLPROBITY (Davis *et al.*, 2004) tools. The AtxA domain identification was based on InterProScan search (Zdobnov & Apweiler, 2001) performed by ProFunc server (Laskowski *et al.*, 2005). A summary of data collection and refinement statistics is given in Tables S1 and S2. Atomic coordinates and structure factors were deposited into the Protein Data Bank as 4R6I.

In vivo AtxA activity assay

To quantify AtxA activity in *B. anthracis*, we employed the *B. anthracis* reporter strain UT376 (*atxA*-null) harboring the transcriptional fusion *lef-lacZ* and plasmids containing *atxA* alleles under control of the hyper-spank promoter (Hammerstrom *et al.*, 2011). Briefly, expression of the *atxA* alleles was induced with IPTG at early log phase (approximately 2 h of growth). Samples were collected at transition phase (approximately 4 h of growth) and assayed for β-galactosidase activity (Hadjifrangiskou & Koehler, 2008).

Preparation of soluble cell lysates from B. anthracis cultures

Co-affinity purification, western blots to determine AtxA level, and cross-linking experiments utilized soluble cell lysates from *B. anthracis* cultures. Cells were cultured in CA medium with bicarbonate and *atxA* expression was induced as described above. Samples from each culture were collected during late exponential phase (4 h). Cells were pelleted

using centrifugation, and washed and resuspended in KTE (10 mM Tris-Cl pH 8.0, 100 mM KCl, 10% ethylene glycol) containing EDTA-free Complete Proteinase Inhibitor (Roche, Indianapolis, IN, USA), or phosphate buffered saline (PBS) with 10 mM EDTA. KTE was used for the co-affinity purification experiments and western blots to determine AtxA protein level, whereas PBS was used for the cross-linking assay. Cell suspensions were added to 0.4 ml of 0.1 mm Zirconia/Silica Beads (BioSpec Products, Bartlesville, OK, USA). The samples were lysed mechanically for 2 min using a Mini BeadBeater (BioSpec Products). Lysates were centrifuged and the soluble cell lysates (supernates) were used immediately in subsequent assays.

Western blotting

The steady-state level of AtxA in *B. anthracis* cultures was determined by subjecting soluble *B. anthracis* cell lysates to immunoblotting followed by densitometry (Hammerstrom *et al.*, 2011). Samples subjected to co-affinity purification or cross-linking were mixed with SDS loading buffer (25% SDS, 62.5 mM Tris-HCl [pH 6.8], 25% glycerol, and 0.01% bromophenol blue), and boiled for 5 min. Proteins were resolved on 10% or 10–15% SDS-PAGE gels and transferred to PVDF membranes (Amersham; GE Healthcare) using a Hoefer transfer unit (Hoefer, Holliston, MA, USA) in 10 mM CAPS pH 11.0, containing 10% methanol. Membranes were blocked overnight in TBS-T (20 mM Tris base, 137 mM NaCl, 0.1% Tween 20 [pH 7.6]) containing 5% non-fat dry milk and subsequently treated with primary antibodies (α-AtxA, α-RNA polymerase β subunit [Santa Cruz Biotechnology, Santa Cruz, CA, USA], α-THE His-HRP [Genscript, Piscataway, NJ] and α-FLAG M2 [Sigma Aldrich]) in TBS-T. After washing with TBS-T, membranes were treated with the corresponding secondary antibody as appropriate (goat α-rabbit–HRP conjugate or goat α-mouse-HRP conjugate [Bio-Rad]). Blots were developed with SuperSignal West Dura Chemiluminescent Substrate (Thermo Scientific, Waltham, MA).

Co-affinity purification

Soluble cell lysates from cultures of *B. anthracis atxA*-null strains expressing AtxA-His, a FLAG-tagged variant of AtxA, or GFP-FLAG were incubated with NTA-Ni resin to bind the AtxA-His protein (Qiagen). AtxA-His and any associated proteins were eluted with imidazole and analyzed by western blot to detect His-tagged and FLAG-tagged proteins as described previously (Hammerstrom *et al.*, 2011).

Protein crosslinking

Crosslinking was performed as described previously (Hammerstrom *et al.*, 2011). Briefly, soluble cell lysates from *B. anthracis* strains expressing AtxA variants were mixed with 400 μM bis(maleimido)hexane (BMH, Thermo Scientific) or the DMSO control by end-over-end rotation at 4°C for 2 h. The reaction was quenched with 40 μM cysteine and cross-linked AtxA multimers were visualized using SDS-PAGE and western blot analysis.

India ink exclusion

Capsulated cells were visualized using an India ink exclusion assay. Briefly, capsule synthesis in induced by culturing cells in NBY medium with 0.8% sodium bicarbonate and

5% atmospheric CO_2 to the late exponential phase of growth (Green *et al.*, 1985). Samples were mixed with India ink on a microscope slide and examined at 1,000× magnification using a Nikon Eclipse TE2000-U microscope (Nikon, Melville, NY). Images were taken by using Metamorph (Imaging Series 6.1) software (Molecular Devices, Sunnyvale, CA).

Supplementary Material

Refer to Web version on PubMed Central for supplementary material.

Acknowledgments

We thank all members of the Structural Biology Center at Argonne National Laboratory for their help in conducting X-ray diffraction data collection. We acknowledge the contributions of Amy Ford, Jason Rall, and Kerrie Thomason for help with mutant construction. We are grateful to Edward Nikonowicz for critical reading of the manuscript.

Argonne is operated by UChicago Argonne, LLC, for the U.S. Department of Energy, Office of Biological and Environmental Research under contract DE-AC02-06CH11357. Work by A.J. and J.O. was supported by grants from the NIAID, NIH, Department of Health and Human Services, Contracts HHSN272200700058C and HHSN272201200026C. Work by T.M.K., T.G.H, L.B.H., and M.C.S. was supported by Award Number R01 AI033537 from the National Institute of Allergy and Infectious Diseases to T.M.K. T.G.H. was also supported during a portion of this work by a training fellowship from the Keck Center Computational and Structural Biology in Biodefense Training Program of the Gulf Coast Consortia (NIH Grant No. 1 T32 AI065396).

References

Adams PD, Grosse-Kunstleve RW, Hung LW, Ioerger TR, McCoy AJ, Moriarty NW, Read RJ, Sacchettini JC, Sauter NK, Terwilliger TC. PHENIX: building new software for automated crystallographic structure determination. Acta Crystallogr D Biol Crystallogr. 2002; 58:1948–1954. [PubMed: 12393927]

Bartkus JM, Leppla SH. Transcriptional regulation of the protective antigen gene of *Bacillus anthracis*. Infection and Immunity. 1989; 57:2295–2300. [PubMed: 2501216]

Ben-Zeev E, Fux L, Amster-Choder O, Eisenstein M. Experimental and computational characterization of the dimerization of the PTS-regulation domains of BglG from *Escherichia coli*. Journal of Molecular Biology. 2005; 347:693–706. [PubMed: 15769463]

Bera AK, Zhu J, Zalkin H, Smith JL. Functional dissection of the *Bacillus subtilis* pur operator site. Journal of Bacteriology. 2003; 185:4099–4109. [PubMed: 12837784]

Bertani G. Studies on lysogenesis. I. The mode of phage liberation by lysogenic *Escherichia coli*. Journal of Bacteriology. 1951; 62:293–300. [PubMed: 14888646]

Bourgogne A, Drysdale M, Hilsenbeck SG, Peterson SN, Koehler TM. Global effects of virulence gene regulators in a *Bacillus anthracis* strain with both virulence plasmids. Infection and immunity. 2003; 71:2736–2743. [PubMed: 12704148]

Cachat E, Barker M, Read TD, Priest FG. A *Bacillus thuringiensis* strain producing a polyglutamate capsule resembling that of *Bacillus anthracis*. FEMS Microbiology letters. 2008; 285:220–226. [PubMed: 18549401]

Casabon I, Couture M, Vaillancourt K, Vadeboncoeur C. Kinetic studies of HPr, HPr(H15D), HPr(H15E), and HPr(His approximately P) phosphorylation by the *Streptococcus salivarius* HPr(Ser) kinase/phosphorylase. Biochemistry. 2009; 48:10765–10774. [PubMed: 19824696]

Cataldi A, Fouet A, Mock M. Regulation of pag gene expression in *Bacillus anthracis*: use of a *pag-lacZ* transcriptional fusion. FEMS Microbiology Letters. 1992; 77:89–93. [PubMed: 1459423]

Chaffin DO, Mentele LM, Rubens CE. Sialylation of Group B streptococcal capsular polysaccharide is mediated by *cpsK* and is required for optimal capsule polymerization and expression. Journal of Bacteriology. 2005; 187:4615–4626. [PubMed: 15968073]

Chiang C, Bongiorni C, Perego M. Glucose-dependent activation of *Bacillus anthracis* toxin gene expression and virulence requires the carbon catabolite protein CcpA. Journal of Bacteriology. 2011; 193:52–62. [PubMed: 20971911]

Collaborative Computational Project N. The CCP4 suite: programs for protein crystallography. Acta Crystallogr D Biol Crystallogr. 1994; 50:760–763. [PubMed: 15299374]

Dai Z, Koehler TM. Regulation of anthrax toxin activator gene (*atxA*) expression in *Bacillus anthracis*: temperature, not CO_2/bicarbonate, affects AtxA synthesis. Infection and Immunity. 1997; 65:2576–2582. [PubMed: 9199422]

Dai Z, Sirard JC, Mock M, Koehler TM. The *atxA* gene product activates transcription of the anthrax toxin genes and is essential for virulence. Molecular Microbiology. 1995; 16:1171–1181. [PubMed: 8577251]

Dale JL, Raynor MJ, Dwivedi P, Koehler TM. *cis*-Acting elements that control expression of the master virulence regulatory gene *atxA* in *Bacillus anthracis*. Journal of Bacteriology. 2012; 194:4069–4079. [PubMed: 22636778]

Davis IW, Murray LW, Richardson JS, Richardson DC. MOLPROBITY: structure validation and all-atom contact analysis for nucleic acids and their complexes. Nucleic Acids Research. 2004; 32:W615–619. [PubMed: 15215462]

Drysdale M, Bourgogne A, Hilsenbeck SG, Koehler TM. *atxA* controls *Bacillus anthracis* capsule synthesis via *acpA* and a newly discovered regulator, *acpB*. Journal of Bacteriology. 2004; 186:307–315. [PubMed: 14702298]

Emsley P, Cowtan K. Coot: model-building tools for molecular graphics. Acta Crystallogr D Biol Crystallogr. 2004; 60:2126–2132. [PubMed: 15572765]

Eschenfeldt WH, Makowska-Grzyska M, Stols L, Donnelly MI, Jedrzejczak R, Joachimiak A. New LIC vectors for production of proteins from genes containing rare codons. Journal of Structural and Functional Genomics. 2013; 14:135–144. [PubMed: 24057978]

Fouet A, Mock M. Differential influence of the two *Bacillus anthracis* plasmids on regulation of virulence gene expression. Infection and immunity. 1996; 64:4928–4932. [PubMed: 8945528]

Gorrec F, Palmer CM, Lebon G, Warne T. Pi sampling: a methodical and flexible approach to initial macromolecular crystallization screening. Acta Crystallogr D Biol Crystallogr. 2011; 67:463–470. [PubMed: 21543849]

Graille M, Zhou CZ, Receveur-Brechot V, Collinet B, Declerck N, van Tilbeurgh H. Activation of the LicT transcriptional antiterminator involves a domain swing/lock mechanism provoking massive structural changes. The Journal of Biological Chemistry. 2005; 280:14780–14789. [PubMed: 15699035]

Green BD, Battisti L, Koehler TM, Thorne CB, Ivins BE. Demonstration of a capsule plasmid in *Bacillus anthracis*. Infection and Immunity. 1985; 49:291–297. [PubMed: 3926644]

Hadjifrangiskou M, Koehler TM. Intrinsic curvature associated with the coordinately regulated anthrax toxin gene promoters. Microbiology. 2008; 154:2501–2512. [PubMed: 18667583]

Hammerstrom TG, Roh JH, Nikonowicz EP, Koehler TM. *Bacillus anthracis* virulence regulator AtxA: oligomeric state, function and CO_2-signalling. Molecular Microbiology. 2011; 82:634–647. [PubMed: 21923765]

Himmel S, Grosse C, Wolff S, Schwiegk C, Becker S. Structure of the RBD-PRDI fragment of the antiterminator protein GlcT. *Acta crystallographica*. Section F, Structural Biology and Crystallization Communications. 2012; 68:751–756.

Holm L, Rosenstrom P. Dali server: conservation mapping in 3D. Nucleic Acids Research. 2010; 38:W545–549. [PubMed: 20457744]

Hondorp ER, Hou SC, Hause LL, Gera K, Lee CE, McIver KS. PTS phosphorylation of Mga modulates regulon expression and virulence in the Group A *Streptococcus*. Molecular Microbiology. 2013; 88:1176–1193. [PubMed: 23651410]

Hondorp ER, Hou SC, Hempstead AD, Hause LL, Beckett DM, McIver KS. Characterization of the Group A *Streptococcus* Mga virulence regulator reveals a role for the C-terminal region in oligomerization and transcriptional activation. Molecular Microbiology. 2012; 83:953–967. [PubMed: 22468267]

Hondorp ER, McIver KS. The Mga virulence regulon: infection where the grass is greener. Molecular Microbiology. 2007; 66:1056–1065. [PubMed: 18001346]

Horton RM, Hunt HD, Ho SN, Pullen JK, Pease LR. Engineering hybrid genes without the use of restriction enzymes: gene splicing by overlap extension. Gene. 1989; 77:61–68. [PubMed: 2744488]

Joyet P, Derkaoui M, Poncet S, Deutscher J. Control of *Bacillus subtilis mtl* operon expression by complex phosphorylation-dependent regulation of the transcriptional activator MtlR. Molecular Microbiology. 2010; 76:1279–1294. [PubMed: 20444094]

Koehler TM, Dai Z, Kaufman-Yarbray M. Regulation of the *Bacillus anthracis* protective antigen gene: CO_2 and a *trans*-acting element activate transcription from one of two promoters. Journal of Bacteriology. 1994; 176:586–595. [PubMed: 8300513]

Krissinel E, Henrick K. Inference of macromolecular assemblies from crystalline state. Journal of Molecular Biology. 2007; 372:774–797. [PubMed: 17681537]

Laskowski RA, Watson JD, Thornton JM. ProFunc: a server for predicting protein function from 3D structure. Nucleic Acids Research. 2005; 33:W89–93. [PubMed: 15980588]

Lee SG, Krishnan HB, Jez JM. Structural basis for regulation of rhizobial nodulation and symbiosis gene expression by the regulatory protein NolR. Proceedings of the National Academy of Sciences of the United States of America. 2014; 111:6509–6514. [PubMed: 24733893]

Lei J, Li LF, Su XD. Crystal structures of phosphotransferase system enzymes PtxB (IIB(Asc)) and PtxA (IIA(Asc)) from *Streptococcus mutans*. Journal of Molecular Biology. 2009; 386:465–475. [PubMed: 19135450]

Marrero R, Welkos SL. The transformation frequency of plasmids into *Bacillus anthracis* is affected by adenine methylation. Gene. 1995; 152:75–78. [PubMed: 7828932]

McIver KS, Heath AS, Green BD, Scott JR. Specific binding of the activator Mga to promoter sequences of the *emm* and *scpA* genes in the Group A *Streptococcus*. Journal of Bacteriology. 1995; 177:6619–6624. [PubMed: 7592441]

McIver KS, Myles RL. Two DNA-binding domains of Mga are required for virulence gene activation in the Group A *Streptococcus*. Molecular Microbiology. 2002; 43:1591–1601. [PubMed: 11952907]

Mignot T, Mock M, Fouet A. A plasmid-encoded regulator couples the synthesis of toxins and surface structures in *Bacillus anthracis*. Molecular Microbiology. 2003; 47:917–927. [PubMed: 12581349]

Minor W, Cymborowski M, Otwinowski Z, Chruszcz M. HKL-3000: the integration of data reduction and structure solution--from diffraction images to an initial model in minutes. Acta Crystallogr D Biol Crystallogr. 2006; 62:859–866. [PubMed: 16855301]

Murshudov GN, Vagin AA, Dodson EJ. Refinement of macromolecular structures by the maximum-likelihood method. Acta Crystallogr D Biol Crystallogr. 1997; 53:240–255. [PubMed: 15299926]

Narayanan A, Kumar S, Evrard AN, Paul LN, Yernool DA. An asymmetric heterodomain interface stabilizes a response regulator-DNA complex. Nat Commun. 2014; 5:3282. [PubMed: 24526190]

Njoroge JW, Nguyen Y, Curtis MM, Moreira CG, Sperandio V. Virulence meets metabolism: Cra and KdpE gene regulation in enterohemorrhagic *Escherichia coli*. mBio. 2012; 3:e00280–00212. [PubMed: 23073764]

Pflughoeft KJ, Sumby P, Koehler TM. *Bacillus anthracis sin* locus and regulation of secreted proteases. Journal of Bacteriology. 2011; 193:631–639. [PubMed: 21131488]

Ravel J, Jiang L, Stanley ST, Wilson MR, Decker RS, Read TD, Worsham P, Keim PS, Salzberg SL, Fraser-Liggett CM, Rasko DA. The complete genome sequence of *Bacillus anthracis* Ames "Ancestor". Journal of Bacteriology. 2009; 191:445–446. [PubMed: 18952800]

Ribardo DA, McIver KS. Defining the Mga regulon: Comparative transcriptome analysis reveals both direct and indirect regulation by Mga in the Group A *Streptococcus*. Molecular Microbiology. 2006; 62:491–508. [PubMed: 16965517]

Rosenbaum G, Alkire RW, Evans G, Rotella FJ, Lazarski K, Zhang RG, Ginell SL, Duke N, Naday I, Lazarz J, Molitsky MJ, Keefe L, Gonczy J, Rock L, Sanishvili R, Walsh MA, Westbrook E, Joachimiak A. The Structural Biology Center 19ID undulator beamline: facility specifications and protein crystallographic results. J Synchrotron Radiat. 2006; 13:30–45. [PubMed: 16371706]

Saile E, Koehler TM. Control of anthrax toxin gene expression by the transition state regulator *abrB*. Journal of Bacteriology. 2002; 184:370–380. [PubMed: 11751813]

Sambrook, JRD. Molecular cloning: a laboratory manual. Cold Spring Harbor, NY: Cold Spring Harbor Laboratory Press; 2001.

Schmalisch MH, Bachem S, Stulke J. Control of the *Bacillus subtilis* antiterminator protein GlcT by phosphorylation. Elucidation of the phosphorylation chain leading to inactivation of GlcT. The Journal of Biological Chemistry. 2003; 278:51108–51115. [PubMed: 14527945]

Schnetz K, Stulke J, Gertz S, Kruger S, Krieg M, Hecker M, Rak B. LicT, a *Bacillus subtilis* transcriptional antiterminator protein of the BglG family. Journal of Bacteriology. 1996; 178:1971–1979. [PubMed: 8606172]

Shuman S. Vaccinia DNA topoisomerase I promotes illegitimate recombination in *Escherichia coli*. Proceedings of the National Academy of Sciences of the United States of America. 1989; 86:3489–3493. [PubMed: 2542933]

Sirard JC, Guidi-Rontani C, Fouet A, Mock M. Characterization of a plasmid region involved in *Bacillus anthracis* toxin production and pathogenesis. International Journal of Medical Microbiology : IJMM. 2000; 290:313–316. [PubMed: 11111904]

Sirard JC, Mock M, Fouet A. The three *Bacillus anthracis* toxin genes are coordinately regulated by bicarbonate and temperature. Journal of Bacteriology. 1994; 176:5188–5192. [PubMed: 8051039]

Solano-Collado V, Lurz R, Espinosa M, Bravo A. The pneumococcal MgaSpn virulence transcriptional regulator generates multimeric complexes on linear double-stranded DNA. Nucleic Acids Research. 2013; 41:6975–6991. [PubMed: 23723245]

Strauch MA, Ballar P, Rowshan AJ, Zoller KL. The DNA-binding specificity of the *Bacillus anthracis* AbrB protein. Microbiology. 2005; 151:1751–1759. [PubMed: 15941984]

Stulke J, Arnaud M, Rapoport G, Martin-Verstraete I. PRD--a protein domain involved in PTS-dependent induction and carbon catabolite repression of catabolic operons in bacteria. Molecular Microbiology. 1998; 28:865–874. [PubMed: 9663674]

Thorne CB, Belton FC. An agar-diffusion method for titrating *Bacillus anthracis* immunizing antigen and its application to a study of antigen production. Journal of General Microbiology. 1957; 17:505–516. [PubMed: 13481332]

Tobisch S, Stulke J, Hecker M. Regulation of the *lic* operon of *Bacillus subtilis* and characterization of potential phosphorylation sites of the LicR regulator protein by site-directed mutagenesis. Journal of Bacteriology. 1999; 181:4995–5003. [PubMed: 10438772]

Tortosa P, Declerck N, Dutartre H, Lindner C, Deutscher J, Le Coq D. Sites of positive and negative regulation in the *Bacillus subtilis* antiterminators LicT and SacY. Molecular Microbiology. 2001; 41:1381–1393. [PubMed: 11580842]

Tsvetanova B, Wilson AC, Bongiorni C, Chiang C, Hoch JA, Perego M. Opposing effects of histidine phosphorylation regulate the AtxA virulence transcription factor in *Bacillus anthracis*. Molecular Microbiology. 2007; 63:644–655. [PubMed: 17302798]

van Tilbeurgh H, Le Coq D, Declerck N. Crystal structure of an activated form of the PTS regulation domain from the LicT transcriptional antiterminator. The EMBO Journal. 2001; 20:3789–3799. [PubMed: 11447120]

Walsh MA, Dementieva I, Evans G, Sanishvili R, Joachimiak A. Taking MAD to the extreme: ultrafast protein structure determination. Acta Crystallogr D Biol Crystallogr. 1999; 55:1168–1173. [PubMed: 10329779]

Welkos S, Little S, Friedlander A, Fritz D, Fellows P. The role of antibodies to *Bacillus anthracis* and anthrax toxin components in inhibiting the early stages of infection by anthrax spores. Microbiology. 2001; 147:1677–1685. [PubMed: 11390699]

Wenzel M, Altenbuchner J. The *Bacillus subtilis* mannose regulator, ManR, a DNA-binding protein regulated by HPr and its cognate PTS transporter ManP. Molecular Microbiology. 2013; 88:562–576. [PubMed: 23551403]

Wilson AC, Hoch JA, Perego M. Two small c-type cytochromes affect virulence gene expression in *Bacillus anthracis*. Molecular Microbiology. 2009; 72:109–123. [PubMed: 19222757]

Wittekind M, Reizer J, Deutscher J, Saier MH, Klevit RE. Common structural changes accompany the functional inactivation of HPr by seryl phosphorylation or by serine to aspartate substitution. Biochemistry. 1989; 28:9908–9912. [PubMed: 2515891]

Yanisch-Perron C, Vieira J, Messing J. Improved M13 phage cloning vectors and host strains: nucleotide sequences of the M13mp18 and pUC19 vectors. Gene. 1985; 33:103–119. [PubMed: 2985470]

Zdobnov EM, Apweiler R. InterProScan--an integration platform for the signature-recognition methods in InterPro. Bioinformatics. 2001; 17:847–848. [PubMed: 11590104]

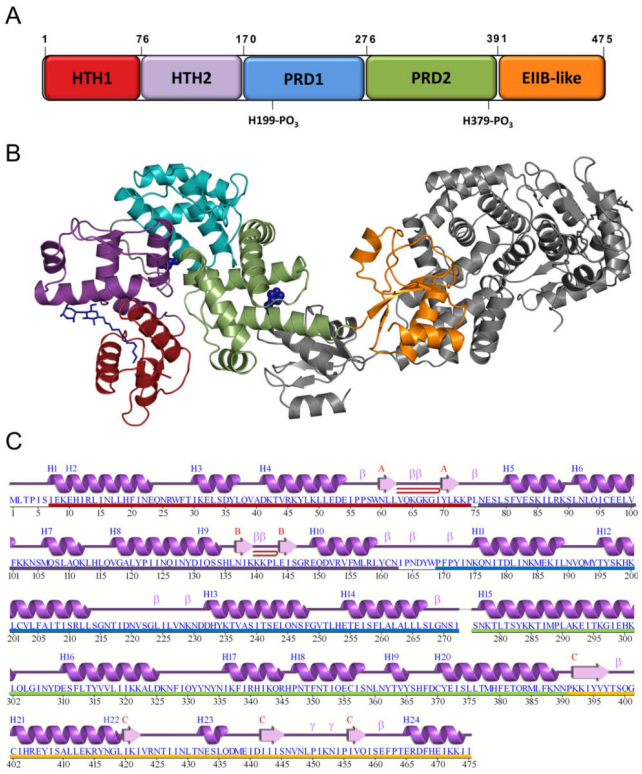

Fig. 1. AtxA modular structure

A) Linear representation of AtxA functional domains showing phosphorylated residues. B) Modular three-dimensional structure of the AtxA dimer as deduced from the crystal structure. The biological dimer is formed by chain A and its symmetry-related molecule. The predicted DNA-binding domains, PRD1, PRD2, and the EIIB-like domain are shown in different colors in one subunit of the dimer. The other subunit is shown in grey. The histidines of the phosphorylation/mutation sites are shown as blue spheres. N-dodecyl-β-D-maltoside molecules are shown as sticks in blue/grey. C) Secondary structure of the AtxA protein based on PDBSum server. α-helices are labelled as H1, H2, … H24 and β-strands by their sheets as A, B and C. Structural motifs β-turns, γ-turns and β-hairpins are marked as β, γ and ⊃, respectively. Predicted domains are marked as lines above the amino-acid sequence in colors corresponding to A and B.

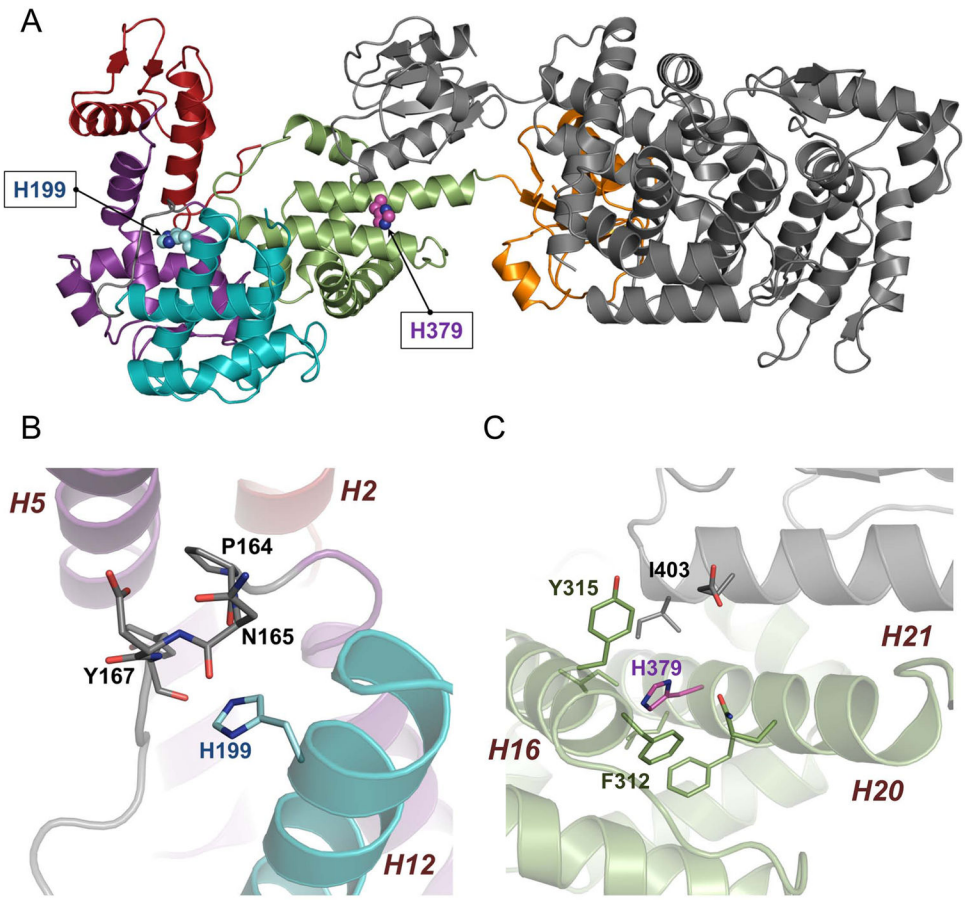

Fig. 2. Locations of histidines, H199 and H379, inside the AtxA protein

A) A general placement of histidines in the protein dimer. B) H199 (in blue/dark blue) and the interacting residues of the linker are shown as sticks. C) H379 (in magenta/dark blue) and surrounding residues are shown as sticks. Helices are marked as *H#* in italics.

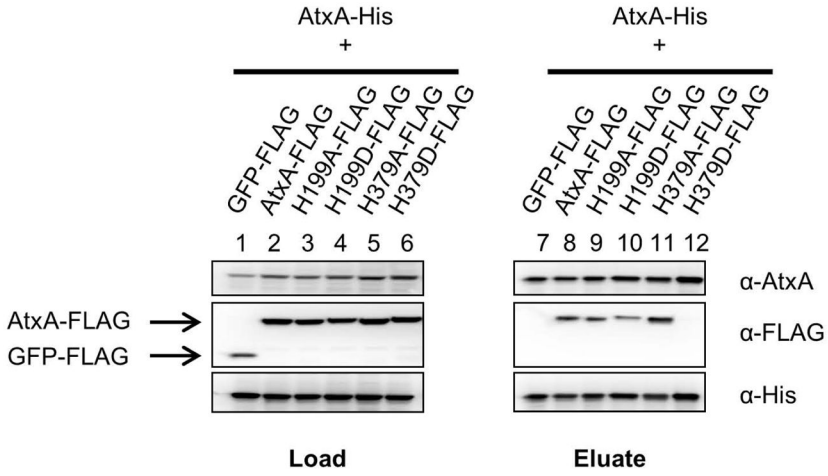

Fig. 3. Co-affinity purification of AtxA proteins with altered phosphorylation sites

Lysates from cultures of UT376 (*atxA*-null mutant) containing AtxA-His (pUTE991), AtxA-FLAG (pUTE992) with H199 or H379 mutations, or GFP-FLAG (pUTE1013) were mixed as indicated and subjected to co-affinity purification using NTA-Ni resin. Western blots of soluble cell lysates (Load, lanes 1–6) and purified proteins (Eluate, lanes 7–12) were probed with α-AtxA, α-FLAG, and α-His antibodies.

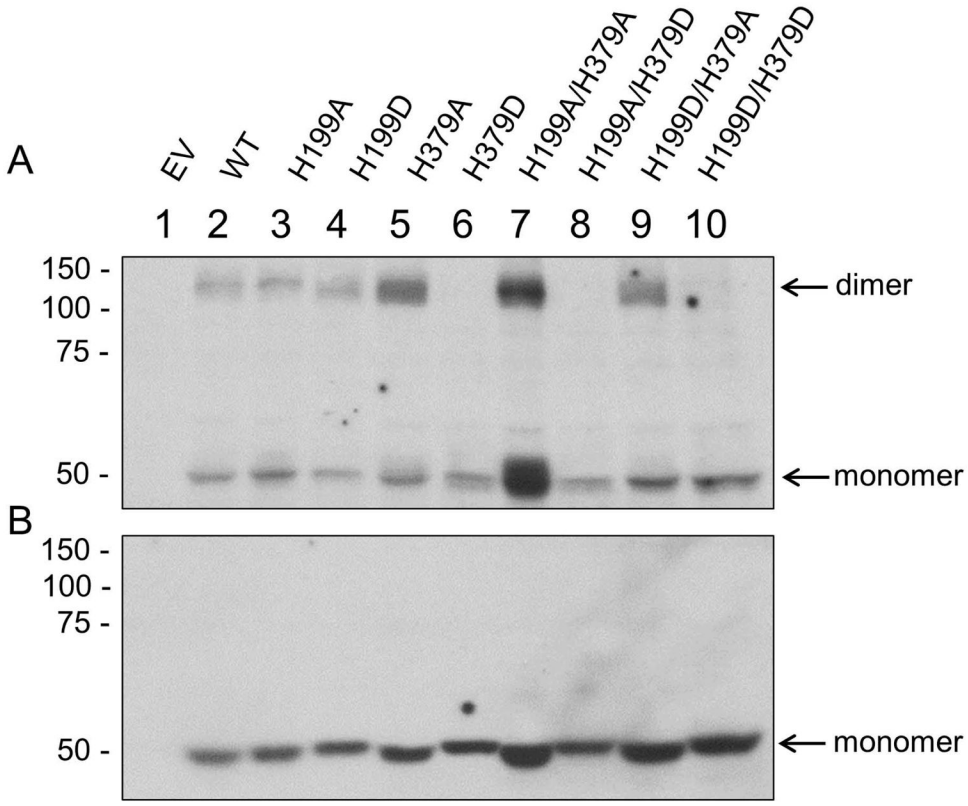

Fig. 4. Crosslinking of AtxA proteins with altered phosphorylation sites

Cultures of *B. anthracis atxA*-null strain (UT376) containing pUTE991 encoding AtxA-His or AtxA-His with mutations in H199 and/or H379 as indicated were induced with IPTG. Soluble cell lysates were prepared from late exponential phase cultures. The lysates were treated with BMH (A) or vehicle only control (B) and subjected to western blotting with α-His-HRP. EV = empty vector. Molecular weights of the protein standards are indicated. Representative data from one of three experiments are shown.

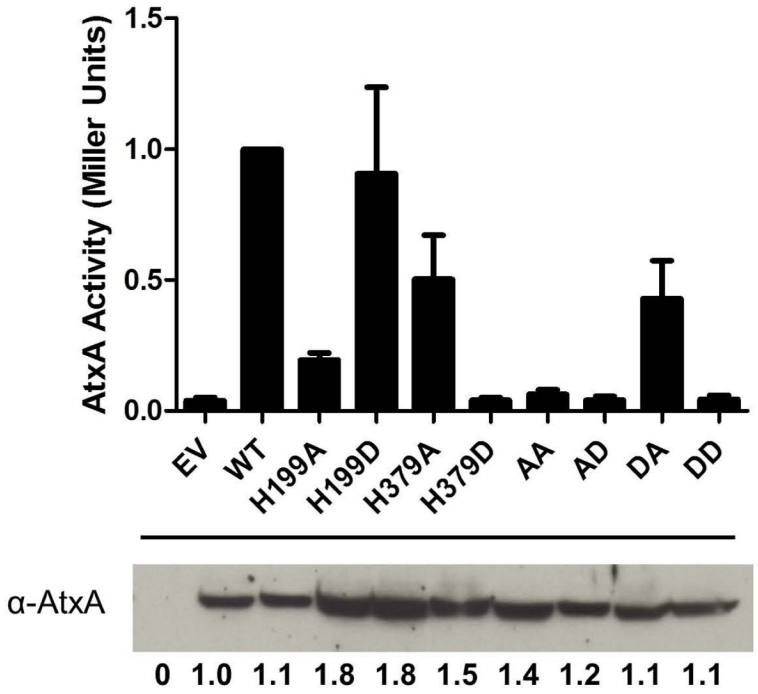

Fig. 5. Activity of AtxA proteins with altered phosphorylation sites

Cultures of the *B. anthracis atxA*-null strain (UT376) containing pUTE658 encoding AtxA or AtxA with mutations in H199 and/or H379 as indicated were induced with IPTG. Double mutants are represented as: AA, H199A H379A; AD, H199A H379D; DA, H199D H379A; DD, H199D H379D. EV = empty vector. Cells were collected from cultures at late exponential phase for AtxA activity assays and western blotting with α-AtxA. AtxA activity was assessed as β-galactosidase activity from a P*lef-lacZ* transcriptional fusion. Activity of mutants was normalized to activity measured for the native protein. Data represent the average of three separate experiments.

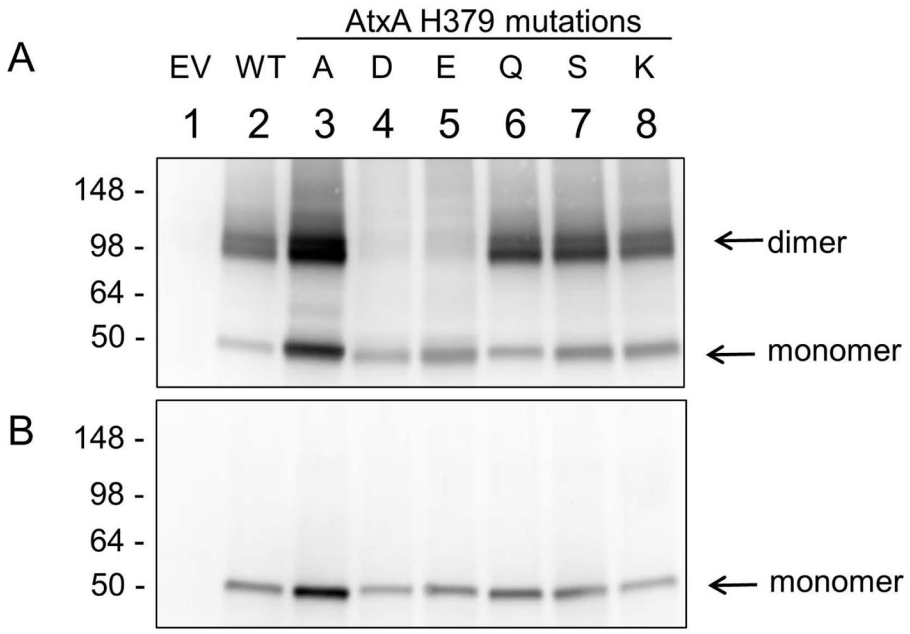

Fig. 6. Crosslinking of AtxA proteins with amino acid substitutions at position 379

Cultures of *B. anthracis atxA*-null strain (UT376) containing pUTE658 encoding AtxA or AtxA with mutations in H379 as indicated were induced with IPTG. Soluble cell lysates were prepared from late exponential phase cultures. The lysates were treated with BMH (A) or vehicle only control (B) and subjected to western blotting with α-AtxA. EV = empty vector. Representative data from one of three experiments are shown.

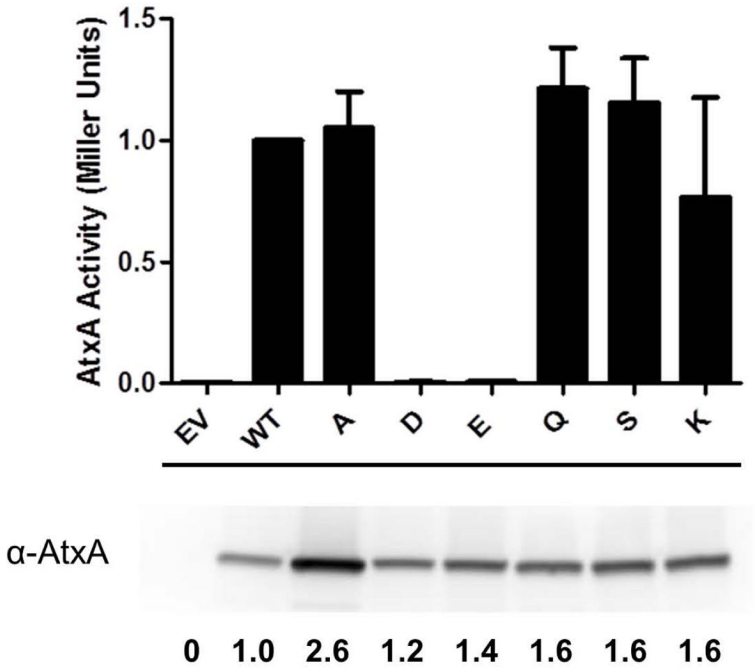

Fig. 7. Activity of AtxA proteins with amino acid substitutions at position 379

Cultures of the *B. anthracis atxA*-null strain (UT376) containing pUTE658 encoding native AtxA or AtxA H379 mutated as shown were induced with IPTG. Cells were collected from late exponential phase cultures for AtxA activity assays and western blotting with α-AtxA. AtxA activity was assessed as β-galactosidase activity from a P*lef-lacZ* transcriptional fusion. Activity of mutants was normalized to activity measured for the native protein. Data represent the average of three separate experiments.

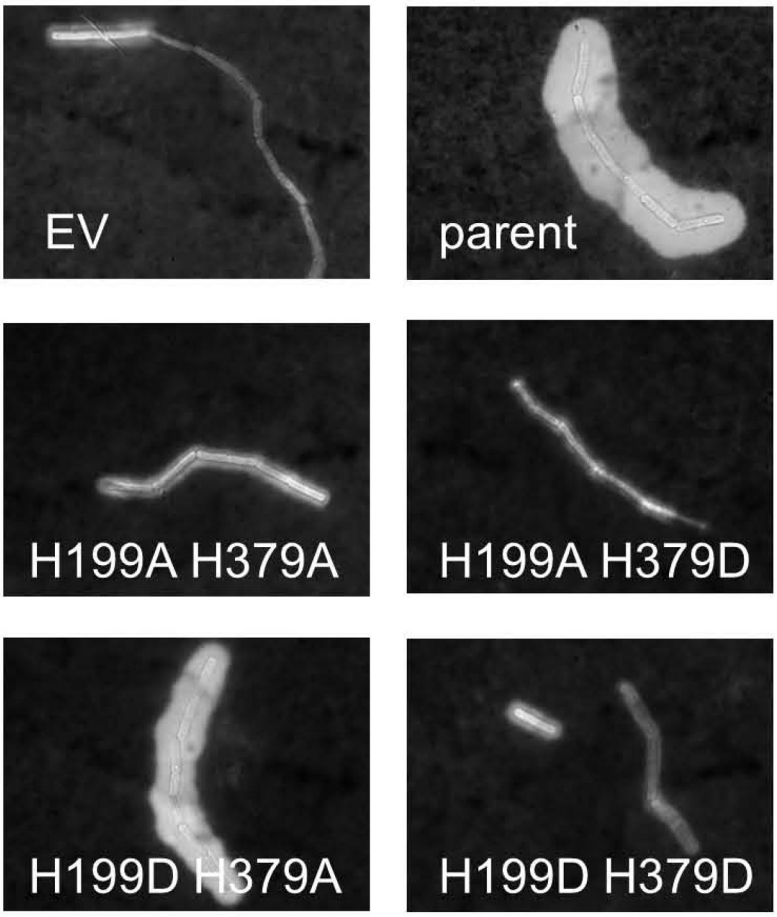

Fig. 8. Capsule production by Ames strain and isogenic mutants expressing phosphomimetic and phosphoablative mutations

Ames *atxA*-null strain (UTA22) containing pUTE658 encoding *atxA* or mutations in H199 and H379 as indicated were induced with IPTG. Samples from cultures at transition phase were added to India ink and imaged using phase-contrast microscopy. EV = UTA22 with empty vector (pUTE657).

Table 1

B. anthracis strains and plasmids used in this study.

Name	Description	Reference
Strains		
ANR-1	*B. anthracis*, Parent strain, pXO1+, pXO2-	(Welkos *et al.*, 2001)
UT376	*B. anthracis* ANR-1 derivative, *lef* promoter–*lacZ* fusion (P*lef-lacZ*) at native *lef* locus, *atxA*-null	(Hammerstrom *et al.*, 2011)
Ames	*B. anthracis*, Parent strain, pXO1+, pXO2+	(Ravel *et al.*, 2009)
UTA22	*B. anthracis* Ames derivative, *atxA*-null	This work
Plasmids		
pHY304	Temperature-sensitive vector used for markerless deletion; Erm^r	(Chaffin *et al.*, 2005)
pMCSG68	Expression vector derived from pMCSG53; contains T7-inducible promoter, N-terminal His6 tag, and TEV Protease cleavage site; Amp^r	(Eschenfeldt *et al.*, 2013)
pJOP2	pMCSG68 containing *his-atxA* (His6 tag on the N- terminus of AtxA)	This work
pUTE657	Expression vector derived from pDR111 and pBC16 with IPTG-inducible P*hyper-spank*; $Spec^r$ Amp^r	(Hammerstrom *et al.*, 2011)
pUTE658	pUTE657 containing *atxA* ribosome binding site and coding region	(Hammerstrom *et al.*, 2011)
pUTE991	pUTE658 containing *atxA-his*	(Hammerstrom *et al.*, 2011)
pUTE992	pUTE658 containing *atxA-FLAG*	(Hammerstrom *et al.*, 2011)
pUTE1013	pUTE657 containing the *gfpmut3a* ribosome binding site and *gfp-FLAG*	(Hammerstrom *et al.*, 2011)